# Development of High Toughness in Austempered Type Ductile Cast Iron and Evaluation of Its Properties

TOSHIRO KOBAYASHI and HIRONOBU YAMAMOTO

In order to increase the toughness of austempered ductile cast irons, we attempted to strengthen the fracture initiation sites such as graphite-matrix interfaces and eutectic cell boundaries in a way of the microsegregation of alloying elements. For instance, the retained austenite which is stable under external stresses may be introduced preferentially into these sites by the addition of Ni, which segregates to a graphite periphery and of Mn, which partitions mainly to eutectic cell boundaries. Following this concept, the effects of various austempering processes on toughness are also investigated. The cast iron alloying with Ni and Mn shows the best fracture toughness when it is heat-treated by either QB′ or B′ process; here, the QB′ means the oil-quenching from an austenite $\gamma$ phase range followed by austempering from a ferrite $\alpha$ plus $\gamma$ range and the B′ means austempering from a ($\alpha$ + $\gamma$) range. In the newly developed iron, there is a mixed microstructure composed of the ferrite, bainitic ferrite, and austenite. Abnormal elongation due to the TRIP effect in the austenite phase is found to have occurred at about 198 K. Moreover, it is shown that this TRIP effect may be caused by the formation of deformation twins.

## I. INTRODUCTION

IT is well known that austempered ductile iron shows good toughness and high strength, because no cementite which is detrimental to the toughness precipitates, while a large amount of retained austenite generally exists in this iron. Therefore, in recent years, the use of austempered ductile irons for structural applications has been increasing.[1–4] From a review of previous investigations on the fracture mechanism for the ductile iron by the present authors,[5,6] it is concluded that fracture will initiate readily not only at the interface between graphite and matrix but also at the eutectic cell boundary.[5,6] Therefore, it is necessary to strengthen these sites from the point of view of higher toughness and strength. It is generally recommended, for example, to lower such elements (*e.g.*, Mn) as will segregate to the eutectic cell boundary and reduce the toughness remarkably.[7] However, in this study, we will utilize such a negative effect positively from the opposite viewpoint. It has been already reported that the QLT treatment in which the low temperature quenching from the ($\alpha$ + $\gamma$) range is inserted intermediately between a conventional quenching and tempering is effective in improving the toughness of 6 to 9 pct Ni ferritic steels for the low temperature use.[8] It has been reported by one of the present authors[8,9] that this treatment is also effective for the ductile iron. In other words, when the low alloyed ductile iron is held in the ($\alpha$ + $\gamma$) range, austenite forming elements diffuse and concentrate into the austenite phase and stabilize this phase; and it is also expected that the induced duplex microstructure enhances the strength as well as the toughness.

In this study, on the basis of the above-mentioned concept, we attempted the following alloy design. The outline of this design is schematically shown in Figure 1. It is already known that silicon concentrates near a graphite nodule and manganese partitions into a eutectic cell boundary. As a result, the austenitizing temperatures ($A_s$, austenitizing starting temperature; $A_f$, austenitizing finishing temperature) will increase near the graphite, while the ones close to the eutectic cell boundary will decrease as is shown in the lower, right drawing in Figure 1. However, an addition of those alloying elements (Ni, Cu, *etc.*) which lower the austenitizing temperature and tend to segregate around graphite nodules, may modify the microstructure into austenite phase near the graphite interface and the eutectic cell boundary only when the alloy is heat-treated at the ($\alpha$ + $\gamma$) range (see the lower, left side drawing in Figure 1). Accordingly, the fracture initiation sites such as a graphite-matrix interface and a eutectic cell boundary may be preferentially

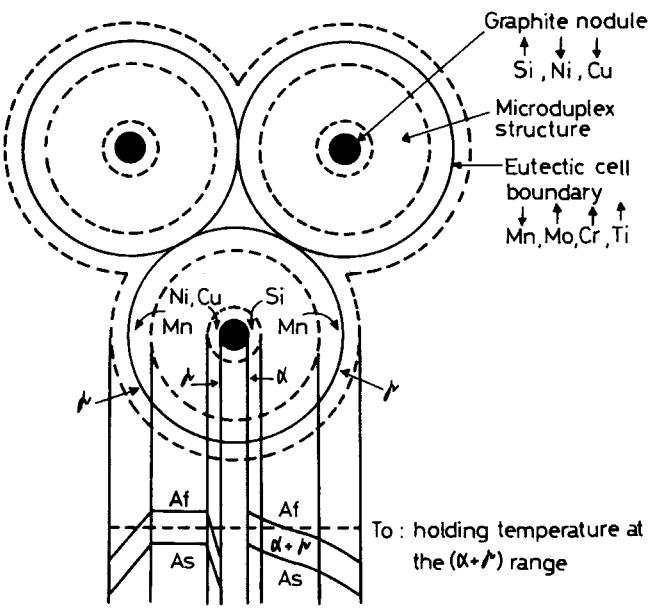


Fig. 1 — Schematic illustration of the microsegregation of alloying elements and phase distributions induced by austempering from the ($\alpha$ + $\gamma$) range. ↑ shows elements which increase $A_1$ point. ↓ shows elements which decrease $A_1$ point.

TOSHIRO KOBAYASHI, Professor, and HIRONOBU YAMAMOTO, Graduate Student, are with the Department of Production Systems Engineering, Toyohashi University of Technology, Tempaku-cho, Toyohashi 440, Japan.

Manuscript submitted October 24, 1986.

modified into the austenite phase which will be stable or show a transformation induced toughening under the existence of external stresses. In this way, the microsegregation of Ni and Mn is expected to be effective improving the mechanical properties of cast irons.

In this study, from these viewpoints, both effects of austempering treatments and alloying elements on the toughening were investigated for the bainitic-type ductile iron. Furthermore, the toughness of some developed irons was evaluated by using static and dynamic elastic-plastic fracture toughness tests. According to the recent fracture mechanics concept, it is said that the toughness should be evaluated in both crack initiation and propagation stages.[10] Crack initiation resistance (static $J_{IC}$ or dynamic $J_d$) and $R$ curve or material tearing modulus ($T_{mat}$) which is a measure of the crack propagation resistance after the crack initiation, were evaluated under both static and dynamic loading conditions. The crack propagation resistance is important from the view of damage tolerant design, and it is known to be sensitive to the microstructure of alloys.[11]

On the other hand, the microstructure resulting from austempering is so complex that there are many problems remaining unsolved. For example, the relationship between the retained austenite and various properties must be clarified, since the microstructure is generally a mixture of bainite and austenite. Also, in this study, attention was directed toward the so-called transformation induced plasticity in the retained austenite phase. An evidence of the transformation induced plasticity (TRIP) phenomenon is found in a newly developed cast iron.

## II. EXPERIMENTAL PROCEDURE

### A. *Material and Heat Treatment*

Chemical composition of the ductile irons used in this study is shown in Table I. Both elements of Ni and Mn were added to irons I to III, while only Mn was added to irons IV and V and only Ni was added to iron VI. The increase of Mn tended to form the undesired cementite, and to suppress its formation, Si content was increased up to 4 pct in iron II. Irons VII to IX were unalloyed, but C and Si contents were varied from a view of the toughness. The measured $A_s$ and $A_f$ temperatures are also shown in Table I.

The heat treatments performed in this study are shown schematically in Figure 2. Symbol B means the conventional austempering, while B′ means the austempering from the ($\alpha$ + $\gamma$) range. B1 and B2 differ in their austenitizing conditions. Symbol Q means the oil-quenching from the $\gamma$ range. In this study, the specimens were coated with a heat-resisting paint and then the austenitizing and the austempering heat treatments were performed in air and a salt bath, respectively.

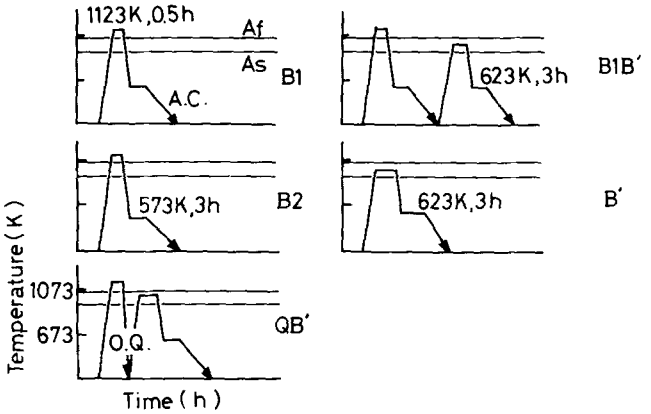


Fig. 2—Schematic representation of heat-treatment processes.

### B. *Instrumented Charpy Impact Test and Fracture Toughness Test*

The heat-treatment conditions and alloying elements suitable for the enhancement of the toughness were chosen using the results of instrumented Charpy test of unnotched specimens. The heat-treated materials were machined into the half-size unnotched Charpy specimen and tested at room temperature by the instrumented Charpy impact testing machine.[11] The fracture toughness ($J_{IC}$, $J_d$), $J_R$ curve, and $T_{mat}$ were evaluated by the DC electrical potential method[4,5] under a static loading condition and also by the instrumented precracked Charpy test with compliance changing rate and key-curve methods that had been developed by Kobayashi *et al.*[12] under a dynamic loading condition. Moreover, this excellent procedure had been proven to be successfully applicable to the ductile iron.[13] The specimens used for the above static and dynamic fracture toughness tests have the standard Charpy size. According to the method of ASTM E813 they are fatigue-precracked so that $a_0/W = 0.6$ ($a_0$: the initial crack length, $W$: the specimen width).

**Table I. Chemical Composition (Mass Pct) and Transformation Temperature (K) of Test Irons**

| Iron | C | Si | Mn | Ni | P | S | Cr | Mg | As | Af |
|---|---|---|---|---|---|---|---|---|---|---|
| I | 2.48 | 1.965 | (0.74) | (3.8) | — | 0.013 | 0.02 | 0.0435 | 963 | 1083 |
| II | 2.50 | (4.08) | (0.89) | (3.9) | — | 0.09 | 0.03 | 0.048 | 1023 | 1153 |
| III | 3.11 | 2.28 | (0.61) | (3.53) | 0.056 | 0.017 | 0.04 | 0.051 | 1103 | 1123 |
| IV | 2.44 | 2.09 | (0.81) | 0.037 | — | 0.012 | 0.01 | 0.040 | 1013 | 1118 |
| V | 3.21 | 1.98 | (0.62) | 0.06 | 0.050 | 0.019 | 0.03 | 0.042 | 1053 | 1073 |
| VI | 2.43 | 1.76 | 0.23 | (3.77) | 0.017 | 0.009 | 0.02 | 0.045 | 1003 | 1083 |
| VII | 2.41 | 1.92 | 0.28 | 0.00 | 0.019 | 0.008 | — | 0.043 | 1063 | 1123 |
| VIII | 3.25 | 3.00 | 0.22 | 0.00 | 0.022 | 0.007 | — | 0.051 | 1063 | 1153 |
| IX | 3.79 | 2.18 | 0.17 | 0.06 | 0.017 | 0.007 | 0.01 | 0.029 | 993 | 1023 |

*Circled number shows a noteworthy content of alloying element in each iron.

C. *Tensile Test*

The tensile test was carried out using an Instron machine on the specimen with the diameter and the gage length of 4 and 20 mm, respectively. This test was carried out in a liquid cooling medium of the temperatures between 298 K and 77 K, changing strain rates in the range from $4 \times 10^{-4}$ to $3.2 \times 10^{-2}$/sec (in most cases $4 \times 10^{-4}$/sec was used). The volume fraction of the retained austenite was determined by the X-ray method, and the microsegregation of alloying elements was examined by using the electron probe X-ray microanalyzer (EPMA). Also the fracture surface and the microstructure were observed by the scanning electron microscopy (SEM) and the transmission electron microscopy (TEM).

## III. EXPERIMENTAL RESULTS AND DISCUSSION

A. *Effect of Austempering Condition on Toughness and Strength*

Heat-treatment conditions in Figure 2 were decided from the results of some preliminary experiments which are summarized as follows. Higher toughness was observed when the austenitizing was performed for a short time at the lower temperatures of the austenite range. It was also confirmed that many irons showed the better toughness when austempered from the ($\alpha + \gamma$) range (see Figure 3). This result was encouraging for the present design of cast irons utilizing the heat treatments and the microsegregations of elements.

Figure 4 shows the change of various properties with austempering times. In the first stage of austempering, the retained austenite is unstable and transforms easily to a martensite during cooling from the austempering temperature as a result of the insufficient carbon enrichment. It is said that the amount of bainitic ferrite saturates to a certain value to be estimated from the thermodynamics.[14] In the same way, the amount of retained austenite reaches a maximum and then cementite precipitates. The toughness is reduced by the precipitation of cementite. Therefore, the absorbed energy shows a maximum, in many cases, at the peak of the amount of retained austenite.[4]

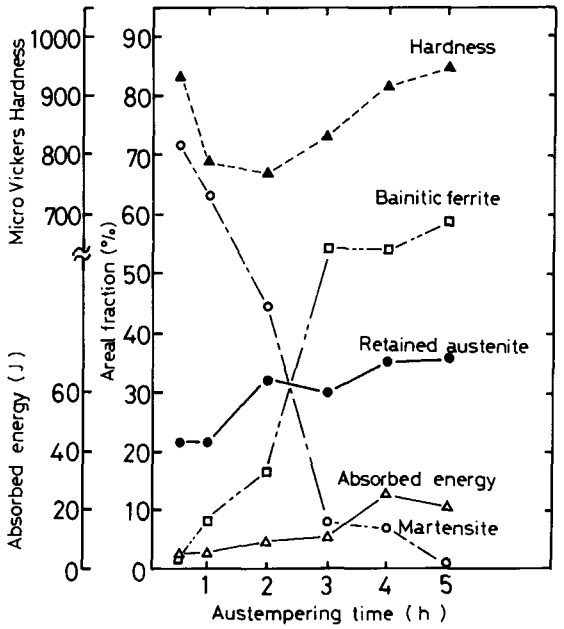


Fig. 4—Change of absorbed energy, hardness of martensite, and areal fraction of constituents of iron I by austempering time at 623 K (austenitizing condition: 1123 K, 0.5 h).

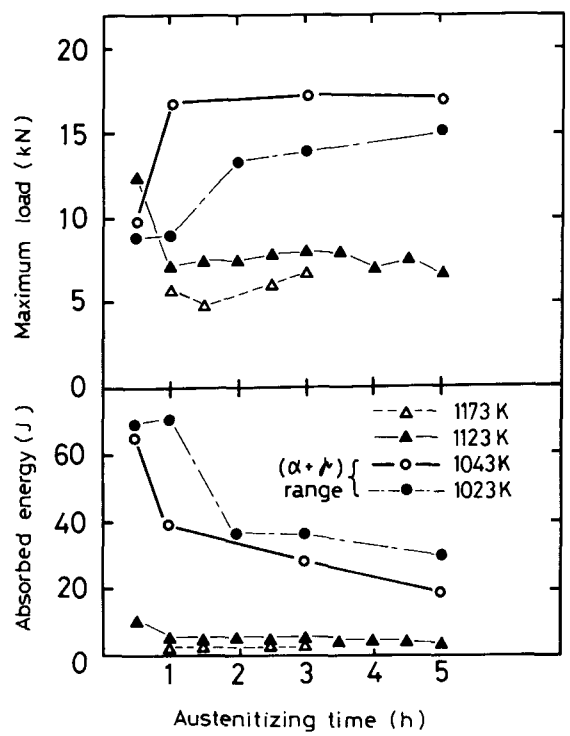


Fig. 3—Change of impact properties of iron I by austenitizing time.

B. *Effects of Alloying Elements and Heat Treatment*

The results of the half-size unnotched Charpy impact test on the variously heat-treated irons are shown in Figure 5. Compared to the conventional heat treatment (B1 or B2), the toughness is improved for the QB′ treatment, which is the pre-quenching from the $\gamma$ phase range to refine the prestructure and subsequent austempering from the ($\alpha + \gamma$) range, and also for the B′ treatment, which is the austempering from the ($\alpha + \gamma$) range.

The relationship between absorbed energy and maximum fracture load obtained from the instrumented Charpy impact test of various irons is shown in Figure 6. It was found from

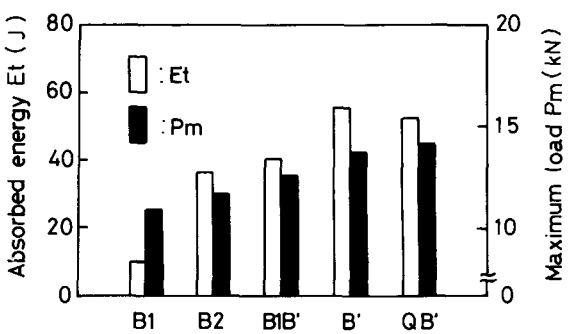


Fig. 5—Change of impact properties by various heat-treatment processes in iron I.

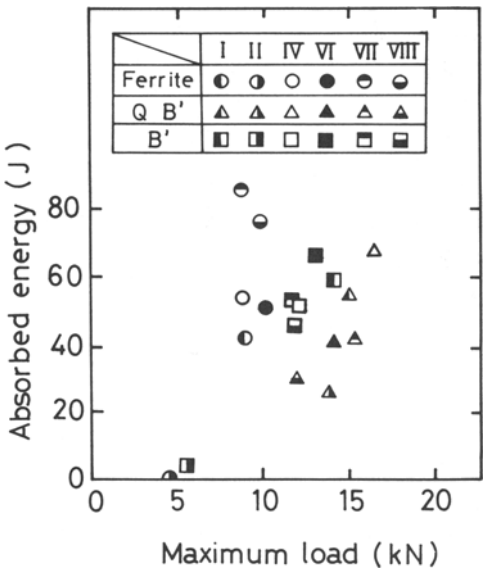


Fig. 6—Relationship between absorbed energy and maximum load in various irons.

this figure that the B′ treated iron alloyed with only Mn and the QB′ treated iron alloyed with Ni and Mn showed the best combination of toughness and strength. SEM micrographs of the retained austenite morphology in each heat-treated iron are shown in Figure 7. The retained austenite morphology has a tendency to become finer in the order of B1, B1B′, and QB′ treatments. It is considered that the toughness increases with the refinement of the retained austenite morphology.

This high toughness in the QB′ treated iron is attributable to the following reasons: (1) Refined grain structure and austenite morphology are inherited in the final structure by the prequenching process. (2) Austenite phase is stabilized as the austenite-forming elements are diffused during annealing in the ($\alpha$ + $\gamma$) temperature range. (3) Ferrite phase also improves its toughness by the high temperature annealing in the ($\alpha$ + $\gamma$) range.

### C. *Effect of Prior Structure on Toughness*

All the results so far explained were obtained using the irons preliminarily fully-ferritic annealed after casting, because it was expected at first that the experimental analysis would be simplified by such a heat treatment. However, it was also thought that such a treatment might contradict the concept of alloy design utilizing the microsegregation in this study. Therefore, the experiment on the prior-structure effect on the toughness was carried out, and the result is shown in Figure 8. The B′ treated irons with different prior structures such as as-cast bull's eye, ferritic, or pearlitic structure were examined using the instrumented Charpy impact test. The B′ treated structure with bull's eye exhibited a good combination of high strength and toughness.

Microsegregations of Ni and Mn in each prior structure are shown in Figure 9. The results of the microsegregation

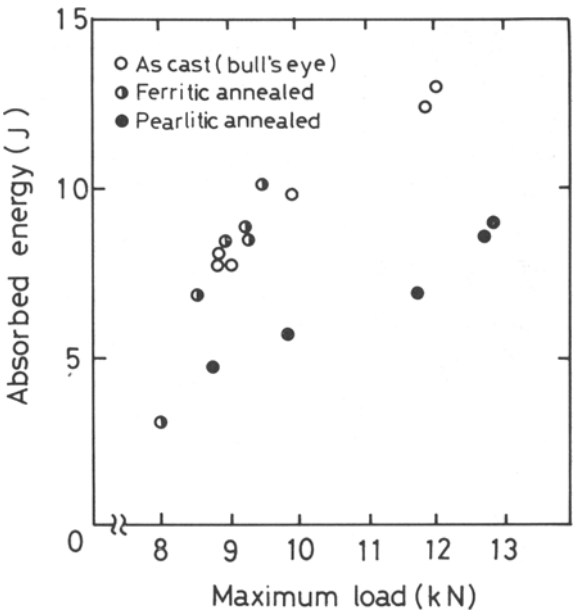


Fig. 8—Relation between absorbed energy and maximum load in specimens variously austempered from each prestructure state (iron II).

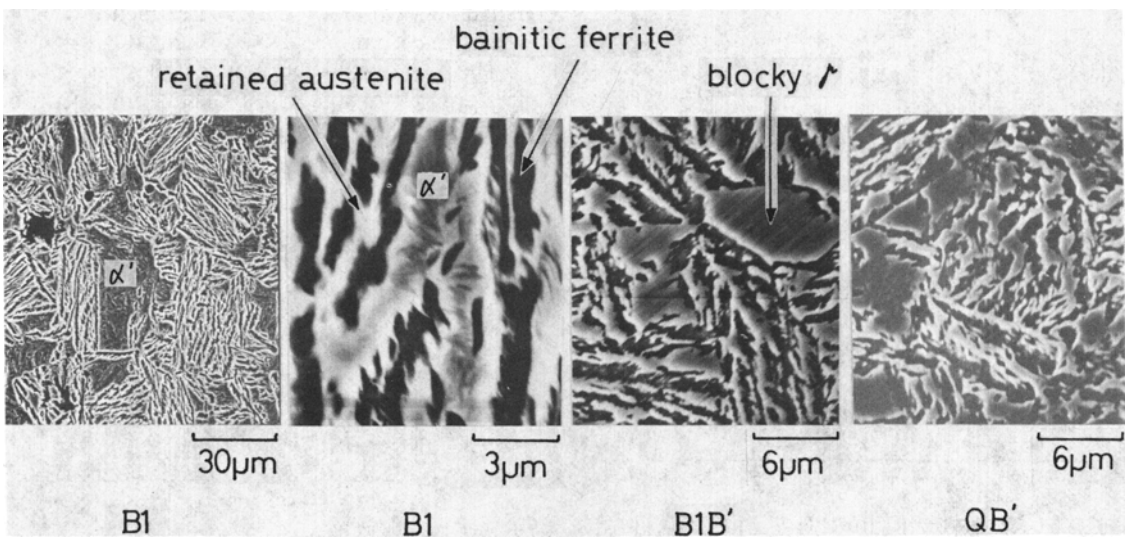


Fig. 7—SEM photographs of the retained austenite morphology in variously heat-treated irons.

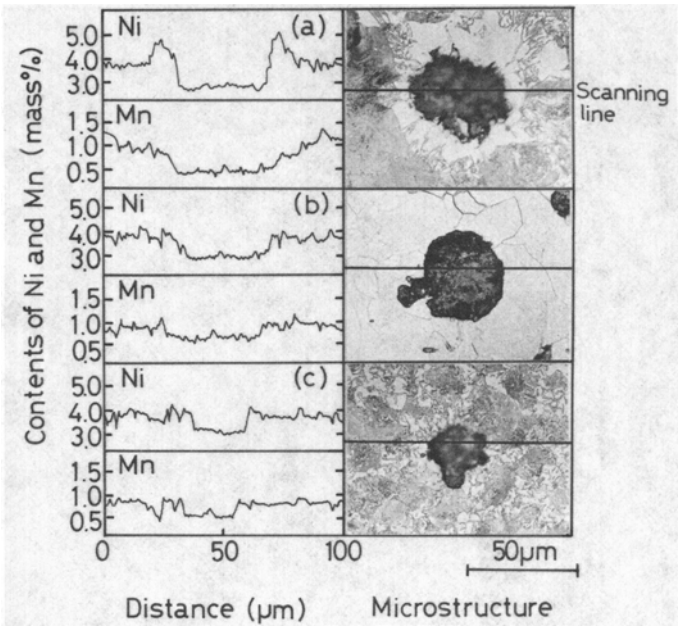


Fig. 9—EPMA result on Ni and Mn distributions and microstructures at various prestructure states (iron II). (*a*) As-cast (bull's eye), (*b*) ferritic annealed, and (*c*) pearlitic annealed.

analysis are different between the as-cast structure and the other prior structures. As shown in Figure 9(a), in the as-cast state, Ni is rich near the graphite nodule and Mn is rich at the eutectic cell boundary in the pearlite. The microsegregations of Ni and Mn in the austempered irons, which showed high toughness in Figure 8, are given in Figure 10. The iron austempered from the as-cast state has mostly inherited a microsegregation character. Moreover, microdistributions of Ni and Mn elements in the austenite and ferrite phases are observed clearly.

A typical TEM micrograph taken by the replica of the bainitic phase is shown in Figure 11. As is found in this micrograph, the filmy, plate-like and blocky retained austenite morphologies are also ascertained.

From the above results, it is expected that our concept for the alloy design is almost satisfactory when the irons, having the as-cast matrix structure (bull's eye structure) and the suitable microsegregations of Ni and Mn, are austempered from the ($\alpha + \gamma$) range. Therefore, the remaining experiments were focused mainly on the QB′ and B′ treated irons and with the as-cast bull's eye prestructure. Some results on the newly developed irons will be explained in the next section.

### D. *Evaluation of Strength and Fracture Toughness Parameters*

Typical microstructures are shown in Figure 12 for the developed irons with a high toughness. Each microstructure consists of the ferrite, the bainite, and the retained austenite. In order to investigate fracture properties on these irons, the elastic-plastic fracture toughness tests were carried out by the electrical potential method under a static loading condition and also by the instrumented precracked Charpy test with compliance changing rate method and key-curve analysis under a dynamic loading condition. This evaluation system has been recently developed by Kobayashi *et al.* and is known as CAI (Computer Aided Instrumented Charpy Impact Testing System).[12,13] The relationship between tensile stress $\sigma_B$ and crack initiation resistance toughness (static $J_{IC}$ and dynamic $J_d$) was obtained as shown in Figure 13. The measured static $J_{IC}$ values satisfied the valid plane strain condition of ASTM E813. Dynamic $J_d$ values also satisfied this condition; however, uncertainty about the validity of dynamic values still remains.[13] The dynamic $J$ values obtained in this study, therefore, are expressed as $J_d$, not as $J_{Id}$. Also, the relationship between $\sigma_B$ and static and dynamic $T_{mat}$ is shown in Figure 14. In this case, the $T_{mat}$ value at

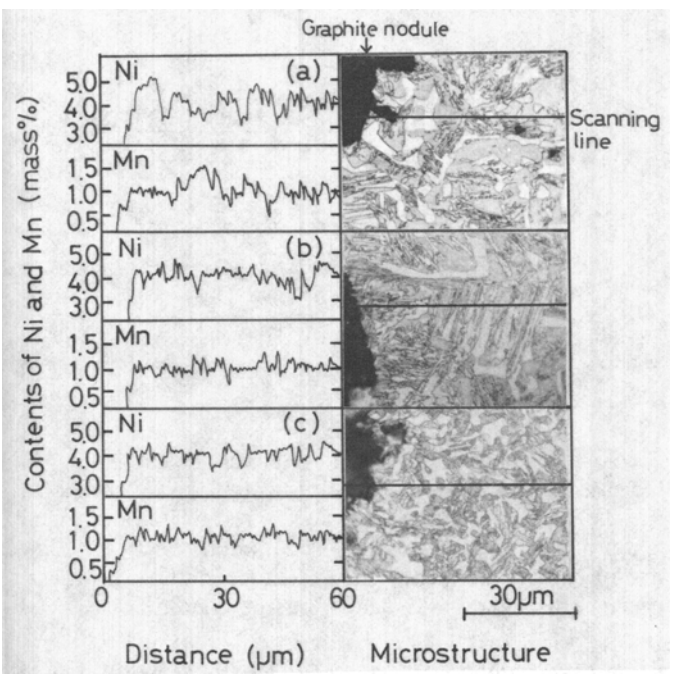


Fig. 10—EPMA result on Ni and Mn distribution and microstructure at variously austempered iron. (*a*) As-cast: 1123 K, 0.5 h–623 K, 3 h A. C. (*b*) Ferrite: 1143 K, 0.5 h–623 K, 3 h A. C. (*c*) Pearlite: 1083 K, 0.5 h–623 K, 3 h A. C.

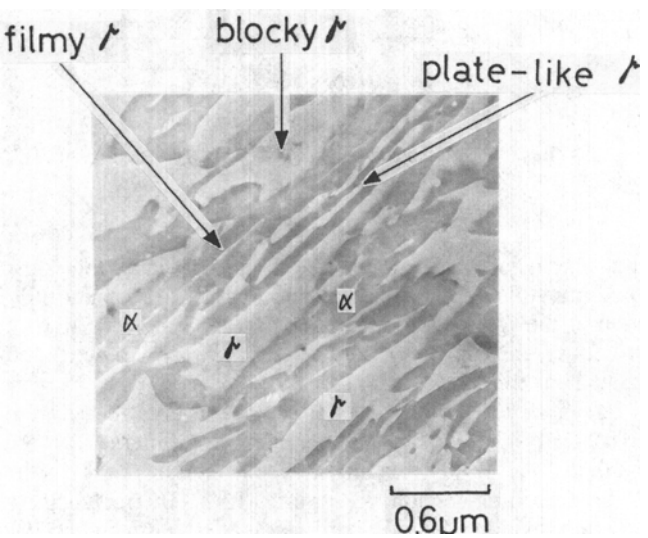


Fig. 11—TEM photograph by replica on the bainitic microstructure (same specimen in Fig. 10(a)). Microconstituents: retained austenite ($\gamma$), bainitic ferrite ($\alpha$).

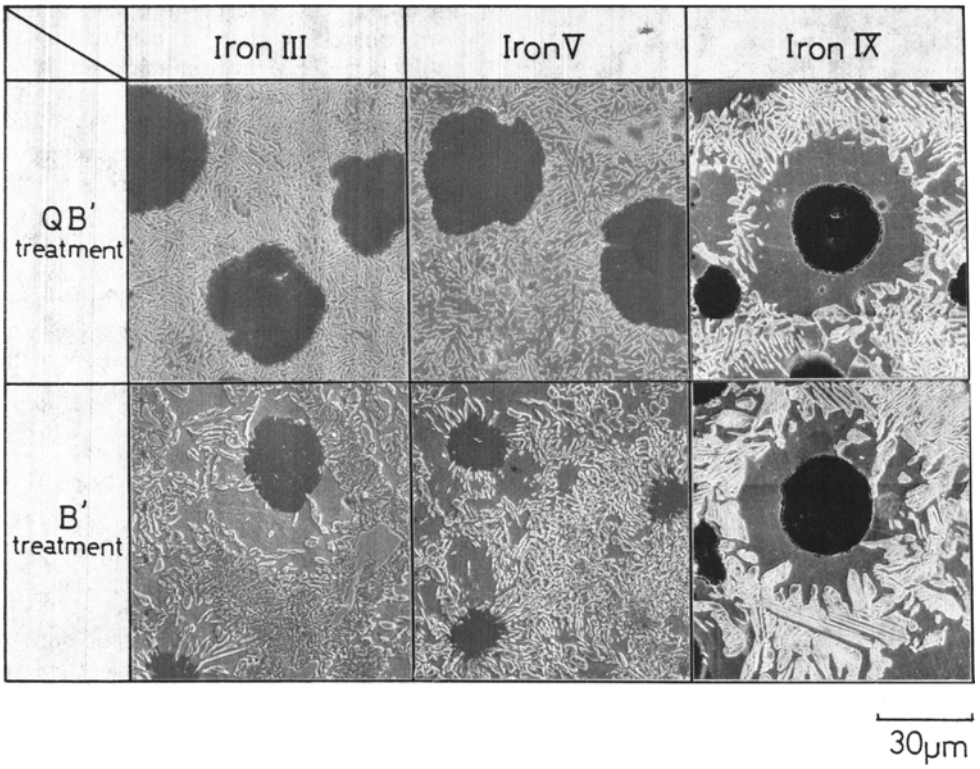


Fig. 12 — SEM photograph of typical microstructures in the developed irons.

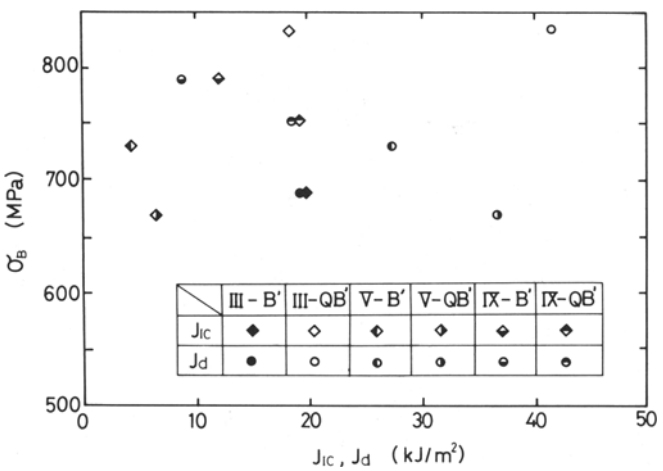


Fig. 13 — Relation between ultimate tensile strength ($\sigma_B$) and $J$ values ($J_{IC}$ and $J_d$).

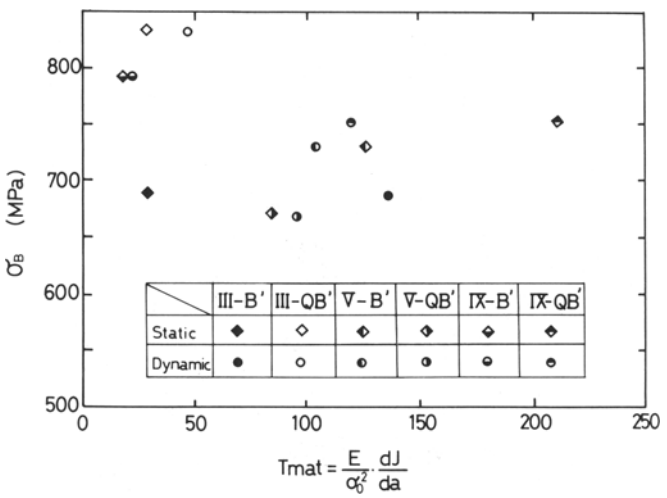


Fig. 14 — Relation between ultimate tensile strength ($\sigma_B$) and $T_{mat}$ (static and dynamic).

crack extension $\Delta a = 1$ mm was plotted, because this is the maximum allowable crack extension value for the determination of the $J_R$ curve in the $J_{IC}$ test method of JSME-S001. Moreover, the limit of $J$ controlled crack growth condition exists near this crack extension.[12]

In Figure 13, the QB′ treated iron III (hereafter referred to as III-QB′) exhibits an excellent combination of the toughness and strength as might be expected from the results in the preceding section. In Figure 14, the B′ treated irons generally exhibit a better combination of strength and propagation toughness than QB′ ones. This high propagation resistance toughness is probably owing to the fact that the path of crack propagation is apt to be deflected by the well-developed duplex structure with relatively coarse grains. In the case of damage tolerant design, therefore, it is expected that the B′ treatment may give a better result. It is also found that propagation toughness $T_{mat}$ is not improved by the addition of Ni or Mn under a static loading condition; however, it is effective under a dynamic loading condition.

### E. *Transformation Induced Plasticity Phenomenon in the Developed Iron*

Temperature dependence of the 0.2 pct proof stress ($\sigma_{0.2}$), tensile strength ($\sigma_B$), and total elongation (El) for the

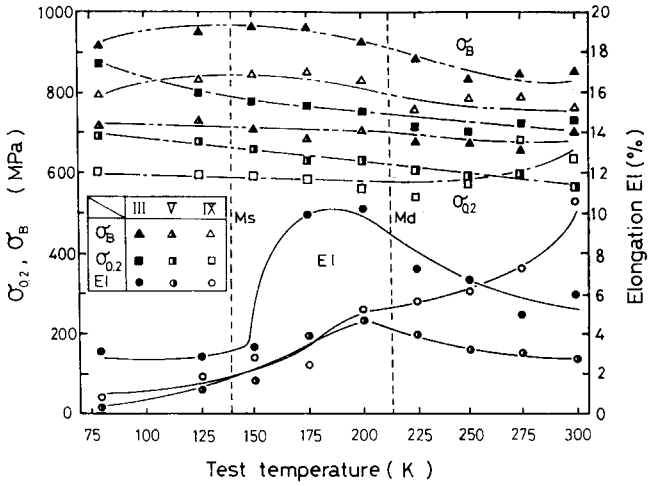


Fig. 15—Temperature dependence of 0.2 pct proof stress ($\sigma_{0.2}$), ultimate tensile strength ($\sigma_B$), and total elongation (El) in static tensile tests of QB′ treated irons.

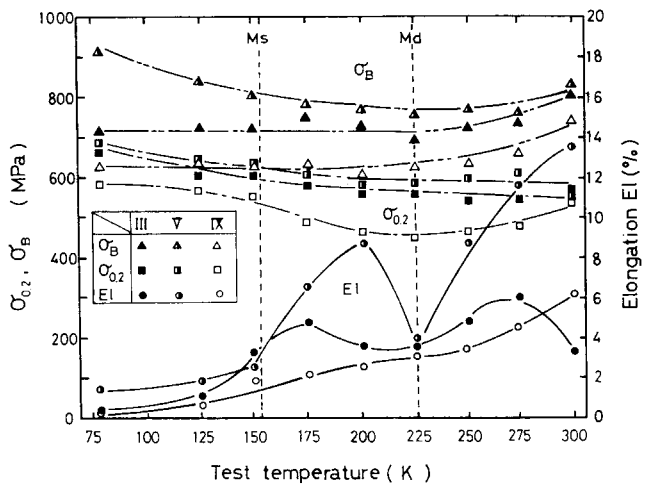


Fig. 16—Temperature dependence of 0.2 pct proof stress ($\sigma_{0.2}$), ultimate tensile strength ($\sigma_B$), and total elongation (El) in static tensile tests of B′ treated irons.

III-QB′ and V-B′ irons are shown in Figures 15 and 16, respectively. It is clearly found that an abnormal elongation appears near 198 K in both irons. The extent of the abnormal elongation temperature range in the III-QB′ or V-B′ iron just corresponded to the temperature range between $M_s$ and $M_d$, where $M_s$ temperature was estimated using the formula reported for stainless steel.[15] Chemical composition of the retained blocky austenite was determined by the EPMA and the result is shown in Table II. Carbon content was estimated from the measurement of lattice constants of the austenite by the X-ray diffraction method. It is ascertained that the retained austenite is enriched with C, Mn, and Ni. On the other hand, $M_d$ temperature for the onset of martensitic transformation by the deformation was estimated following the report that $M_d$ appeared generally 40 to 70 K above the $M_s$ in austenitic ductile irons.[16] The Ni equivalent was also estimated from the formula for stainless steels.[15] It was reported that TRIP tended to appear when $Ni_{eq}$ = 20 to 30. The estimated Ni equivalent in the retained

**Table II. Determined Alloy Content (Mass Pct), $Ni_{eq}$ (Pct), and $M_s$ Temperature (K) of the Retained Austenite Phase in III-QB′ and V-B′ Irons**

| | C | Si | Mn | Ni | $Ni_{eq}$[(1)] | $M_s$[(2)] |
|---|---|---|---|---|---|---|
| III-QB′ | 1.775 | 2.37 | 0.66 | 3.95 | 27.85 | 143.5 |
| V-B′ | 1.82 | 1.93 | 0.84 | 0.07 | 24.56 | 151.1 |

[(1)] $Ni_{eq}$ = Ni + 1.05 × Mn + 0.35 × Si + 12.6 × C (pct)
[(2)] $M_s$ = 550 − 350 × C − 40 × Mn − 17 × Ni + 273 (K)

austenite lies in this range. Therefore, it is assumed that this phenomenon has a feature of TRIP.

On the other hand, the measured strain-hardening exponent was almost constant at 298 K, the temperature above $M_d$, and also at 77 K, the temperature below $M_s$. The variation of strain-hardening exponent with strains was also small at 198 K. For a well-known TRIP caused by the deformation induced martensite, it has been reported that the strain-hardening exponent increases largely with increasing strain.[17] The present result was different from this feature of the TRIP.

The amount of the retained austenite on the fracture surface of the tensile specimen correlated with the total elongation as is shown in Figure 17. The change of the retained austenite content is small around the temperature where a peak exists in the elongation curve. From these results, it is suggested that the mechanism of the phenomenon observed in this study is different in some way from the TRIP caused by the deformation induced martensite. Therefore, thin foils were prepared from the fracture surface of specimens after tensile tests at the peak-elongation temperature and other temperatures and the observation of the retained austenite was carried out using TEM. A typical example is shown in Figure 18. The deformation induced martensite has not been observed in the retained austenite. However, a change in the substructure was observed when compared with the other specimens tested at the other temperature range. This change was strongly suggested to be caused by the deformation twin from the analysis of electron diffraction pattern.

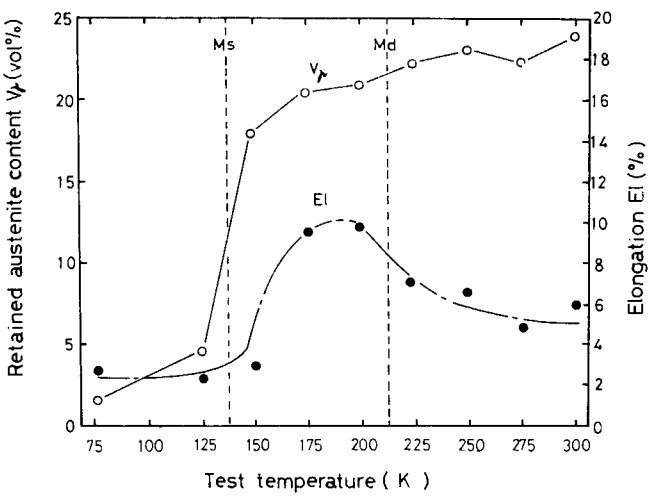


Fig. 17—Temperature change of retained austenite content and total elongation in III-QB′.

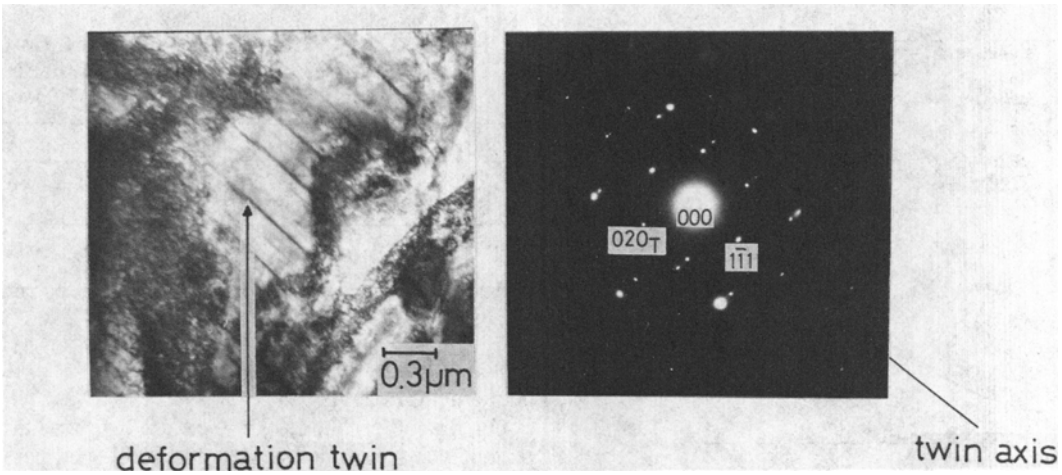


Fig. 18—TEM micrograph showing the deformation twin formed in the retained austenite (III-QB′ tested at 198 K).

It has already been reported that formation of deformation twins or stacking faults is the intermediate stage while the austenite transforms into martensite.[18] It has also been reported that the hardening in the Hadfield steel is due to the work hardening effect by the formation of deformation twins and not by the formation of martensite.[19] In analogy with this case, the TRIP phenomenon observed in this study is probably caused by the formation of the deformation twin. We defined this phenomenon as "the TRIP in a wide sense". On the other hand, the TRIP caused by the transformation induced martensite is defined as "the TRIP in a narrow sense". This phenomenon has already been suggested by one of the present authors on high Mn steels.[20]

The effect of strain rate on the TRIP caused by the deformation twin was also studied. Tensile test was performed at the peak-elongation temperature employing several strain rates in the range between $4 \times 10^{-4}$ and $3.2 \times 10^{-2}$/sec. The elongation decreased with increasing strain rate.

The decreasing rate of elongation with respect to strain rate for the III-QB′ iron was smaller than that for the V-B′ iron, and the absolute value of elongation was larger in the III-QB′ iron. It is considered that this difference is brought about by the difference of phase stabilization in the retained austenite, because the retained austenite in the III-QB′ iron is enriched with both elements Ni and Mn. It is a necessary condition for the transformation toughening that simultaneous progression of transformation or twin formation and fracture should occur in the crack tip process zone. In such a situation, elastic strain energy may be released rapidly by the formation of deformation twins. It will be necessary hereafter, therefore, to clarify the mechanism and to develop a special technique to cause the TRIP even under the high strain rate condition.

Figure 19 is the tensile-properties map in which the newly developed irons are located together with various ordinary ductile irons heat treated and tested in the past by the authors. It is evident that the developed iron has high strength and toughness. We hope that the concept described in this study is utilized in the industry.

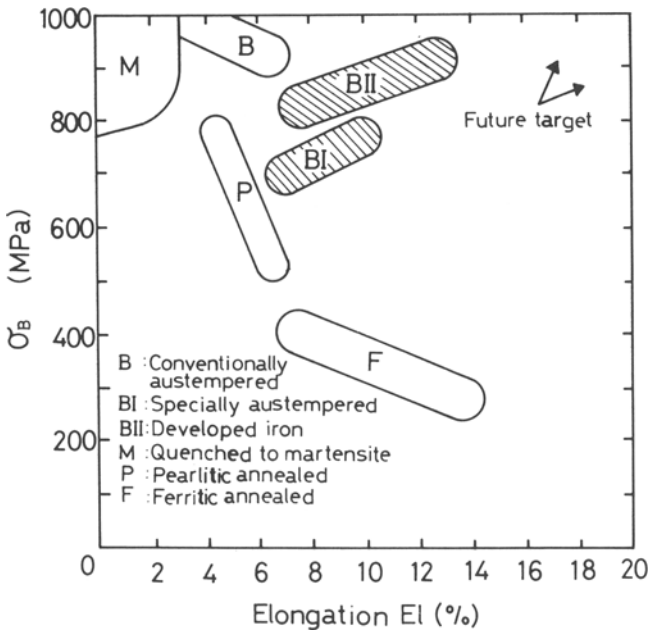


Fig. 19—Summarized comparison of tensile properties among various ductile irons at room temperature.

## IV. CONCLUSION

1. New austempered type low alloyed ductile cast iron has been developed and reported in this study. For the new alloyed iron, the best toughness is obtained when the iron, having the as-cast structure (*i.e.*, bull's eye structure) and the suitable microsegregation of alloying elements Ni and Mn, is heat-treated by the B′ or QB′ treatment. Here, the B′ treatment is the austempering from the ($\alpha + \gamma$) range, and the QB′ treatment is the prequenching from the $\gamma$ range and then followed by B′ treatment.
2. From the results on the toughness under static and dynamic loading conditions, it was concluded that the

QB′ treatment increases the crack initiation resistance ($J_{IC}$ and $J_d$), while the B′ treatment increases the crack propagation resistance ($T_{mat}$) largely in the Ni and Mn alloyed iron.

3. The phenomenon of TRIP was found at about 198 K in the tensile test of the newly alloyed irons, III-QB′ and V-B′. However, this TRIP was different in some way from a well-known TRIP caused by the deformation induced martensite. It was suggested this TRIP was mainly caused by the formation of deformation twins.

## ACKNOWLEDGMENTS

The authors would like to thank Professor M. Morinaga for his critical reading of the manuscript and Dr. M. Niinomi for his discussion and Mr. F. Kawakubo and Y. Takabayashi for their help in the experimental work. They also thank Kurimoto, Ltd. for their financial support of this work.

## REFERENCES

1. J. F. Janowak and R. B. Gundlack: *AFS Trans.*, 1983, vol. 91, p. 377.
2. E. Dorazil, B. Barta, L. Stransky, E. Munsterova, and A. Huvar: *Giesserei-Praxis*, 1982, vol. 19, p. 303.
3. R. B. Gundlack and J. F. Janowak: *Metal Progress*, 1985, vol. 128, p. 19.
4. M. Johansson: *AFS Trans.*, 1977, vol. 85, p. 117.
5. T. Kobayashi: *Kinzoku-Gakkai-hō*, 1983, vol. 45, p. 155.
6. T. Kobayashi and S. Nishi: *Imono (in English)*, 1980, vol. 52, p. 76.
7. Lo-Kan: *Fonderie*, 1977, vol. 367, p. 167.
8. S. Nagashima, T. Ooka, S. Sekino, H. Mimura, T. Fujishima, S. Yano, and H. Sakurai: *Trans. ISIJ*, 1971, vol. 58, p. 402.
9. T. Kobayashi and H. Tachibana: *Trans. JIM*, 1983, vol. 24, p. 281.
10. R. O. Ritchie and A. W. Thompson: *Metall. Trans. A*, 1985, vol. 16A, p. 233.
11. T. Kobayashi: *Eng. Frac. Mech.*, 1984, vol. 19, p. 49.
12. T. Kobayashi, I. Yamamoto, and M. Niinomi: *Eng. Frac. Mech.*, 1986, vol. 24, p. 733.
13. T. Kobayashi, I. Yamamoto, and M. Niinomi: *Proc. 9th Cong. Mat. Testing*, Budapest, 1986, vol. I, p. 75.
14. H. K. D. H. Bhadeshia and D. V. Edmonds: *Met. Sci.*, 1983, vol. 17, p. 411.
15. T. Fujita, H. Misawa, and H. Tsutsumi: *Tetsu-to-Hagané*, 1972, vol. 58, p. 1693.
16. A. Ikenaga and K. Okabayashi: *Imono*, 1980, vol. 52, p. 263.
17. I. Tamura and T. Maki: *Toward Improved Ductility and Toughness*, Climax Mo. Co. Ltd., Japan, 1971, p. 183.
18. C. H. White and P. W. K. Honeycombe: *JISI*, 1962, vol. 202, p. 457.
19. Y. N. Dastur and W. C. Leslie: *Metall. Trans. A*, 1981, vol. 12A, p. 749.
20. T. Kobayashi, W. Yagi, T. Kajino, and Y. Ueda: *Tetsu-to-Hagané*, 1984, vol. 70, p. 861.